A stochastic surrogate Hamiltonian approach of coherent and incoherent exciton transport in the Fenna-Matthews-Olson complex

N. Renaud,[1,a)] M. A. Ratner,[1,b)] and V. Mujica[2,3,c)]
[1]*Northwestern University, Department of Chemistry 2145 Sheridan Road, Evanston, Illinois, 60208-3113, USA*
[2]*Department of Chemistry and Biochemistry, Arizona State University, Tempe, Arizona 85287-1604, USA*
[3]*Center for Nanoscale Materials, Argonne National Laboratory, Argonne, Illinois 60439, USA*

(Received 25 May 2011; accepted 13 July 2011; published online 17 August 2011)

The capture and transduction of energy in biological systems is clearly necessary for life, and nature has evolved remarkable macromolecular entities to serve these purposes. The Fenna-Matthews-Olson (FMO) complex serves as an intermediate to transfer the energy from the chlorosome to the special pairs of different photo systems. Recent observations have both suggested the importance of coherent exciton transport within the FMO and motivated an elegant and appropriate theoretical construct for interpreting these observations. Here we employ a different approach to exciton transport in a relaxing environment, one based on the stochastic surrogate Hamiltonian method. With it, we calculate the quantum trajectories through the FMO complex both for the model involving seven bacteriochlorophylls that has been used before, and for one involving an eighth bacteriochlorophyll, which has been observed in some new and very important structural work. We find that in both systems, efficient energy transfer to the ultimate receptor occurs, but that because of the placement of, and energy relaxation among, the different bacteriochlorophyll subunits in the FMO complex, the importance of coherent oscillation that was discussed extensively for the seven site system is far less striking for the eight site system, effectively because of the weak mixing between the initial site and the remainder of the system. We suggest that the relevant spectral densities can be determinative for the energy transport route and may provide a new way to enhance energy transfer in artificial devices.
 [doi:10.1063/1.3624376]

I. INTRODUCTION

As part of an ongoing discussion of the implications of quantum mechanics in biological processes,[1–3] energy transport in light harvesting compounds was long thought dominated by a classical hopping mechanism from one pigment to another without any quantum weirdness.[4] Very fast dephasing of the quantum propagation along the pigment network was supposed to be responsible for the lack of delocalisation and quantum coherence in the exciton transfer across the system. Recent experiments have proven this assumption wrong. Studying exciton transport in the Fenna-Matthews-Olson (FMO) complex[5] using two-dimensional coherent electronic spectroscopy,[6,7] Engel *et al.* have shown that quantum coherence is preserved up to a picosecond during the relaxation of an initial excited state generated by a femtosecond laser pulse.[8] Many other experiments have led to similar conclusions in different biological compounds[9–11] raising the question: are quantum tricks used to transfer energy efficiently from the antenna, where the photons are captured, to the reaction center where the photosynthesis occurs? Several authors have argued in this direction proposing that the initial exciton might perform a quantum search algorithm among the FMO complex components to transfer energy efficiently[12] or suggesting a relationship between Darwin's theory of evolution and quantum mechanics.[13] Even if these propositions are highly speculative, understanding the details of energy transfer in natural compounds such as the FMO complex could be a first step toward the design of efficient bio-inspired solar cells.[14]

The FMO complex is a made of three identical subunits, each composed of a network of bacterio-chlorophylls (BChl) embedded in a protein environment. The first x-ray characterization of the complex, made in 1975,[5] determined that each subunit contained seven BChl. Recently a eighth BChl has been resolved in the structure, changing a 30 years old view.[17] With seven or eight BChl, the role of the FMO is quite clear: to transfer excitons from the chlorosome to the reaction center. Therefore, exciton propagation over the BChl network is of prime importance to the photosynthesis machinery. This propagation is driven by the excitonic Hamiltonian, $\mathcal{H}_S$, accounting both for the Förster interactions between the pigments and for their respective on-site energies.[16,17] The latter are different from one pigment to another, depending on their local protein environment; these also induce energy relaxation and decoherence onto the coherent propagation.[17] Simulating accurately the combination of the coherent evolution and the relaxation processes is key to understanding excitonic propagation in photosynthetic systems.

Nearly all the methods developed to compute the dynamics of a quantum system interacting with its environment are based on the same strategy: the entire system is

a)Electronic mail: n-renaud@northwestern.edu.
b)Electronic mail: ratner@northwestern.edu.
c)Electronic mail: vmujica@asu.edu.

partitioned into two parts, the principal system, described by the Hamiltonian $\mathcal{H}_S$, and a bath modeling the environment and described by the Hamiltonian $\mathcal{H}_B$.[18] The system and the bath interact through the Hamiltonian $\mathcal{H}_{SB}$. The challenge is then to understand how the system relaxes from an excited state to its thermal state when transferring its excess energy to the bath. Several alternatives to the formal solution given by Nakajima and Zwanzig[19,20] have been developed to permit the computation of this energy relaxation. The Redfield approach is one of the most popular schemes used by the exciton transfer community.[17,21,23] Based on the Born-Markov approximation, this equation supposes that the bath is infinite and memoryless, preventing any energy flow back from the bath to the system. Beside, using perturbation theory, the Redfield approach can lead to physical inconsistencies, such as negative populations, when the interactions between the system and the bath are too strong.[22] The Lindblad equation has been constructed to obtain a semi-group dynamics and, therefore, to ensure that the trace of system's density matrix, $\rho_S(t)$, remains equal to one.[22] However, the derivation of the relaxation operators involved in the Lindblad equation from microscopic arguments is still a challenge.[24] More recent methods try to simulate the dynamics of an open quantum system from a different starting point. The Monte Carlo wave function (MCWF) method,[25] developed in the frame of quantum optics, is based on quantum jumps randomly performed on $\rho_S(t)$ while its propagation is made with a non-Hermitian Hamiltonian. This combination of quantum jumps and non-unitary propagation insures to obtain a trace preserving overall propagation that converges to the Bloch equation for a two-level system. However, the MCWF and its recently proposed non-Markovian generalization[26] require frequent numerical renormalization of the density matrix which leads to difficulties in their physical interpretation. The reduced hierarchy equation approach[27] gives an interesting but rather complex tool to treat wavelike motion and incoherent hopping in the same framework.

The so-called surrogate Hamiltonian (SH) technique[28] assumes that the infinite number of two-level quantum modes comprising the bath, can be truncated to a finite representative number, energetically spanning the typical energy of the system. Combined with efficient grid propagation methods, this approach has been successfully applied to wave function propagation and relaxation in various potential shapes, simulating different physical process from ultrafast pump-probe charge transfer[28] to photodesorption of small molecules.[29] However, this approach deals with a closed system and the energy transfer eventually reaches a recurrence point and flows back from the bath to the system. The SH approach is, therefore, suitable only for short evolution time. An obvious solution to delay the recurrence point is of course to increase the number of bath modes, increasing simultaneously the computational cost. A smarter solution, so-called stochastic surrogate Hamiltonian (SSH), has recently been proposed.[30] Instead of increasing the number of modes, the SSH approach introduces a secondary bath identical to the primary bath and acting such as a sink on the latter. The two baths interact with each other through random swapping of the reduced density matrix (RDM) of their respective quantum modes. Applying this technique to one-dimensional potentials, the SSH approach has given very satisfying results for long evolution time with a very limited number of modes comprising the primary bath and consequently for a fairly decent computational cost.[31] An interesting question is now to know if this new algorithm can be extended in order to be applied to excitonic transfer in photosystems whose Hamiltonians are described on a discrete basis set.

The article is organized as follows: in Sec. II the outline of the SSH algorithm on a discrete basis set is presented. The algorithm is reformulated in terms of quantum jumps instead of swaps, removing the fictional secondary bath. The comparison of the dynamics obtained using the Redfield equation and the SSH in the Markovian limit is made for a two level system. In Sec. III, the SSH approach is applied to a tight-binding model of coherent excitonic transfer in the FMO complex, accounting for the recently discovered eighth pigment. The comparison between these dynamics and the one obtained with only seven pigments is made and leads to new consideration on the role of quantum coherence during this transfer. Finally in Sec. IV, the role of the bath spectral density is considered; under some circumstances, it can entirely dominate the physics.

A. The stochastic surrogate Hamiltonian revisited

To study the relaxation of an open quantum system, its Hamiltonian is divided in three parts: $\mathcal{H} = \mathcal{H}_S + \mathcal{H}_B + \mathcal{H}_{SB}$. Here, $\mathcal{H}_S$ is the Hamiltonian of the system, $\mathcal{H}_B$ that of the bath, and $\mathcal{H}_{SB}$ defines their mutual interactions. In the frame of a tight binding implementation of the SSH algorithm, represented in Fig. 1, the Hamiltonian of the system is defined by

$$\mathcal{H}_S = \sum_{i=a,b,\ldots} e_i |i\rangle\langle i| + \sum_{i\neq j} \alpha_{ij} |i\rangle\langle j|, \tag{1}$$

where e_i is the energy of the $|i\rangle$ state of the system and α_{ij} the coupling strength between state $|i\rangle$ and $|j\rangle$. The basis set $\{|a\rangle, |b\rangle, \ldots\}$ can represent different types of states from molecular orbitals to excitonic states; allowing us to address very different problems while remaining in the same framework. The Hamiltonian of the bath is given by[30]

$$\mathcal{H}_B = \sum_{i=1}^{N} \omega_i \boldsymbol{\sigma}_i^\dagger \boldsymbol{\sigma}_i, \tag{2}$$

where ω_i are the mode energies. The creation and annihilation operators, $\boldsymbol{\sigma}_i^\dagger$ and $\boldsymbol{\sigma}_i$, on the ith bath mode are defined on the total basis set formed by all the bath modes and can be easily calculated using a recursive algorithm.[28] Finally the interaction Hamiltonian between the system and the bath is chosen to simulate electronic relaxation[28] and reads

$$\mathcal{H}_{SB} = \mathcal{R}_S \otimes \sum_{i=1}^{N} \mathcal{J}(\omega_i)(\boldsymbol{\sigma}_i^\dagger + \boldsymbol{\sigma}_i), \tag{3}$$

where $\mathcal{R}_S$ is the relaxation pathways matrix and $\mathcal{J}(\omega_i)$ is the spectral density of the bath, evaluated at the bath-mode frequency ω_i. The $\mathcal{R}_S$ matrix is a key element in the SSH algorithm since it defines the transitions in the energy

relaxation of the system. In the following, this matrix is defined on the eigenbasis set of $\mathcal{H}_S$ to simulate the relaxation between different eigenstates, noted $\{|1\rangle, \ldots, |N\rangle\}$, of the system. Following,[28] the matrix elements $\langle n|\mathcal{R}_S|m\rangle$ and $\langle m|\mathcal{R}_S|n\rangle$ equal 1/2 if the transition between the eigenstates $|n\rangle$ and $|m\rangle$ is allowed. Despite the fact that all the allowed transitions are equivalent in $\mathcal{R}_S$, their respective rates can be very different depending on the value of $\mathcal{J}(\omega)$ at their respective transition frequencies. These three Hamiltonians drive the unitary evolution of the entire system following the solution of the Liouville equation: $\rho(t) = e^{-i\mathcal{H}\frac{t}{\hbar}}\rho(0)e^{i\mathcal{H}\frac{t}{\hbar}}$. Following the SSH approach, quantum jumps are performed at random times. Each jump resets the RDM of one bath mode to its thermal state with a random phase. The RDM of the jth mode is defined on the basis formed by its ground and excited state labeled, respectively, $|0_j\rangle$ and $|1_j\rangle$. If the jth mode jumps, its RDM must be reset to[30]

$$\rho_j^T = \frac{1}{2\cosh(2\Omega_j)} \begin{array}{c} \begin{matrix} |0_j\rangle & |1_j\rangle \end{matrix} \\ \begin{pmatrix} e^{-\Omega_j} & e^{-i\theta} \\ e^{+i\theta} & e^{\Omega_j} \end{pmatrix} \end{array} \tag{4}$$

with $\Omega_j = \hbar\omega_j/2k_bT$, θ_i a random phase factor, and T the temperature of the bath. Thus, a jump rate Γ_j, defined below, and a random number ε_j are associated with each mode. During the evolution, if $\exp(-\Gamma_j\tilde{t}_j) < \varepsilon_j$, the jth mode jumps to its thermal state and a new random number ε_j is given to the mode. Here, $\tilde{t}_j$ is the time elapsed since the last jump of the jth mode. These jumps simulate the energy exchange between the bath modes explicitly treated during the evolution and a larger unresolved environment. The ratio between the jump rate of each mode and its interaction with the system is a key component of the SSH algorithm. The jump rate, Γ_j, of the jth mode is defined by

$$\Gamma_j = \Lambda \times \mathcal{J}(\omega_j), \tag{5}$$

where Λ is chosen according to the lifetime of the bath modes and, therefore, controls the degree of Markovianity of the algorithm.[32] Non-Markovian dynamics arise when the bath is not infinite and can partially excite back the system. Depending on the ratio between the excitation and de-excitation of the system by its interaction with the bath, a given process can be more or less Markovian leading naturally to the idea of degree of Markovianity. This specific aspect of the SSH algorithm would not be addressed in this article and will be the focus of a future publication. Let us just say that for a large value of Λ the bath modes are constantly reset to their thermal state which corresponds to a very short lifetime of the bath. The bath is then equivalent to an infinite sink and the SSH algorithm converges to a Born-Markov approach such as the Redfield equation. On the contrary when Λ is small, the bath modes can reach highly excited states and can eventually give energy back to the system before being reset to their thermal state. This leads to a partial flow back of energy from the bath to the system that is typical of non-Markovian dynamics.[26] The jump operation is performed as follows: each time a bath mode has to be reset the RDM of the system and the RDM of each bath mode are computed from the total density matrix. The RDM of the bath mode that jumps is reset to its thermal state and the total density matrix is recomputed from all the RDMs. Therefore, each jump not only simulates the exchange of energy between the bath modes and the unresolved larger environment but also destroys some coherences in the system due to the coherence to population transfer arising between the system's coherences and the excited state populations of the bath modes. Depending on the interactions between the system and the bath, different coherences of the system may decay with different rates.

Because it involves random events, the SSH algorithm imposes a statistics on the evolution. Thus, the Liouville equation is solved K times, each time being called a realization, and performing quantum jumps in the bath manifold. For each realization, the bath-mode frequencies are chosen, randomly covering the typical energy range of the system. Quantum jumps occur at different times during each realization. The overall dynamics is obtained by computing the mean value of the K realizations and the RDM of the system is calculated by tracing over the bath modes degree of freedom,

$$\rho_S(t) = Tr_B\left[\frac{1}{K}\sum_{k=1}^{K}\rho^{(k)}(t)\right]. \tag{6}$$

The choice of the initial state, $\rho(0)$, has a strong impact on the dynamics. A thermal, correlated initial state between the system and the bath can be obtained propagating an initial guess state in backward imaginary time, reaching the ground state of the entire system.[33] This correlated state avoids the initial artifact in the energy relaxation where the system's energy may increase for very short evolution time.[28] An uncorrelated initial state, defined by: $\rho(0) = \rho_S(0) \otimes \exp(-\mathcal{H}_B/k_BT)$, is widely used in the literature; this choice of initial state is generally justified by the fact that after the excitation, the system is very weakly entangled with the bath. Neglecting the inherent system-bath correlation, this initial state is not physical but is generally suitable for electronic excitation process – it corresponds to excitation in accordance to the Franck-Condon transition.[34] In this article, we will use an uncorrelated initial state where each bath mode is in its thermal state defined by Eq. (4) and the system in a non-stationary excited state, ρ_S^{ex}. Thus the initial state is given by: $\rho(0) = \rho_S^{ex}\bigotimes_{j=1}^{N}\rho_j^T$. That way we ensure that the quantum jumps performed on the bath manifold reset the bath modes to their initial state.

II. DIMER SYSTEM IN THE MARKOVIAN LIMIT

To examine the validity of the SSH approach in a tight binding model, the simple case of a dimer system is presented here. The general form of the system Hamiltonian for such a system is

$$\mathcal{H}_S = \begin{array}{c} \begin{matrix} |a\rangle & |b\rangle \end{matrix} \\ \begin{pmatrix} e_a & \alpha \\ \alpha & e_b \end{pmatrix} \end{array}. \tag{7}$$

In the following the local states will always be labeled as letters and the eigenstates by numbers. Depending on the value of the energies e_i and the coupling strength α, different systems can be studied from heterogeneous molecules[21] to

atoms in a cavity.[26] A frequently used benchmark dimer system consists in a two weakly coupled sites with $\alpha = 10$ meV, and extremely close in energy with $e_b - e_a = 1$ meV which corresponds to typical values for photosynthetic systems. To compute $\mathcal{H}_{SB}$ following Eq. (3), the relaxation matrix $\mathcal{R}_S$ has to be defined. Here we choose to simulate the relaxation from the excited state, $|2\rangle = -\sin(\theta)|a\rangle + \cos(\theta)|b\rangle$, to the ground state $|1\rangle = \cos(\theta)|a\rangle + \sin(\theta)|b\rangle$, of the system where $\theta = 2(\alpha/(e_a - e_b))$. This gives the relaxation matrix,

$$\mathcal{R}_S = \begin{array}{c} \\ |1\rangle \\ |2\rangle \end{array} \begin{array}{c} \begin{array}{cc} |1\rangle & |2\rangle \end{array} \\ \begin{pmatrix} 0 & 1/2 \\ 1/2 & 0 \end{pmatrix} \end{array}. \tag{8}$$

The computation of $\mathcal{H}_{SB}$ also requires the definition of the bath density of states, $\mathcal{J}(\omega)$. Several models are available to define $\mathcal{J}(\omega)$ depending on the type of system studied. One model used in the context of energy transfer in photosynthetic systems, the so-called overdamped Brownian oscillator (OBO),[35] is given by the spectral density,

$$\mathcal{J}(\omega) = 2\lambda \frac{\omega}{\omega^2 + \omega_c^2}, \tag{9}$$

where λ is the reorganization energy and ω_c the cutoff frequency of the bath. Typical values of λ for exciton relaxation in photosynthetic systems lie around 1–10 meV and ω_c is typically around 1–5 ps$^-$. Using these parameters, the dynamics of this dimer system, initially prepared on $|b\rangle$, have been computed following the SSH approach, and also with the Redfield equation for validation. As explained above, the Redfield approach supposes that the bath remains at equilibrium during the evolution. In the SSH frame, this hypothesis requires performing quantum jumps often enough for the bath modes not to be excited. To obtain rapid jump rates following Eq. (5), Λ is chosen as: $\Lambda = 1.05$.[30] The population of the state $|a\rangle$, obtained with both approaches, is represented in Fig. 2 for different values of λ: $\lambda = 2$, 5, 7, and 10 meV, with $\omega_c = 1.5$ ps$^-$ and for a temperature of 300 K. The SSH dynamics has been solved using 6 modes in the bath and performing 100 realizations with a 0.5 fs time step. The good

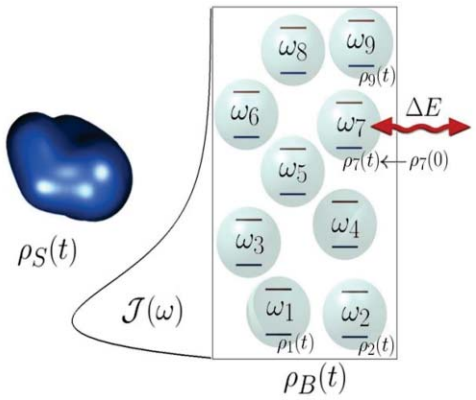

FIG. 1. Graphical representation of the SSH model. The coupling between the system and each bath mode is proportional to the bath spectral density, $\mathcal{J}(\omega)$, at the frequency of the corresponding mode. At random times, the RDM of a given bath mode, here the seventh, is reset to its initial thermal state. These jumps simulate the energy exchange between the bath modes and an unresolved larger environment and progressively destroy the coherence.

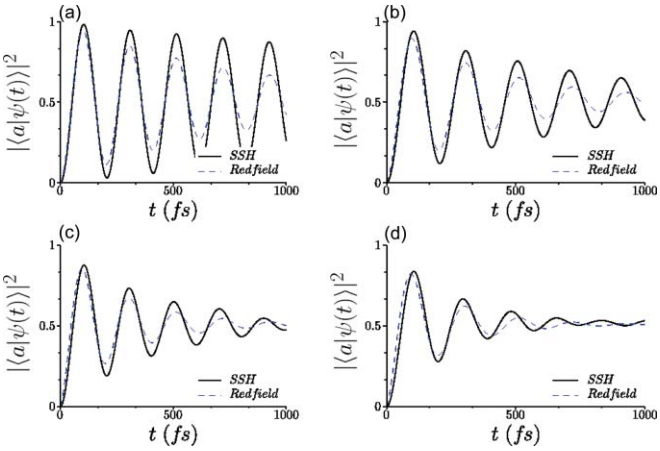

FIG. 2. Dynamics of a dimer system computed with the SSH approach (plain) and the Redfield equation (dashed). The dimer is initially prepared in $|b\rangle$ and is characterized by $e_b - e_a = 1$ meV and $\alpha = 10$ meV. The cutoff frequency of the bath is set at $\omega_c = 1.5$ ps^{-1} and the reorganization energy is: $\lambda = 2$ meV (a), 5 meV (b), 7 meV (c), and 10 meV (d). The temperature of the bath was set to 300 K. The SSH dynamics has been solved using 6 modes, 100 realizations, and for $\Lambda = 1.05$.

agreement seen between the two methods suggests the ability of the tight-binding SSH algorithm to deal with this limit. On top of the slightly different relaxation rate obtained with the SSH and the Redfield approach, a difference in the oscillation frequency also appears. In the SSH approach, the eigenvalues of the system are explicitly modified by its interactions with the bath, that naturally leads to a modification of its internal oscillation frequency. Note that the agreement between the Redfield equation and the SSH depends on the jump rate Λ. For smaller values of Λ, these two methods give significantly different results since the Born-Markov approximation is no longer valid within the SSH algorithm. However, in the limit of the slow jump rate, the SSH and the recently developed non-markovian quantum jump approach gives very similar results. As pointed out in the early stage of the SSH algorithm development, a value of Λ slightly above 1 gives the fastest relaxation rate since the jumps occur when the excited states of the bath modes are strongly populated and, therefore, remove a maximal amount of energy from the system.[30]

The populations of the two states gives information on how the energy is relaxed during the evolution. Starting from $|b\rangle$, the system reaches a state where both $|a\rangle$ and $|b\rangle$ are almost equally populated. However, it is impossible to know from the populations if this asymptotic state is a coherent state, such as $1/\sqrt{2}(|a\rangle \pm |b\rangle)$ or a mixed state. The Bloch sphere representation[36] can be used to get a global picture of the dynamics and understand the nature of the final state. The trajectory of the system in the Bloch representation is constructed from its RDM as

$$T = \begin{cases} \mathcal{X}(t) = \rho_{aa}(t) - \rho_{bb}(t), \\ \mathcal{Y}(t) = 2\,\Im[\rho_{ab}(t)], \\ \mathcal{Z}(t) = 2\,\Re[\rho_{ab}(t)], \end{cases} \tag{10}$$

where $\rho_{ij}(t) = \langle i|\rho_S(t)|j\rangle$. Mapping both the population difference ($\mathcal{X}(t)$) and the evolution of the coherences ($\mathcal{Y}(t)$ and $\mathcal{Z}(t)$) on the sphere, the Bloch representation provides a

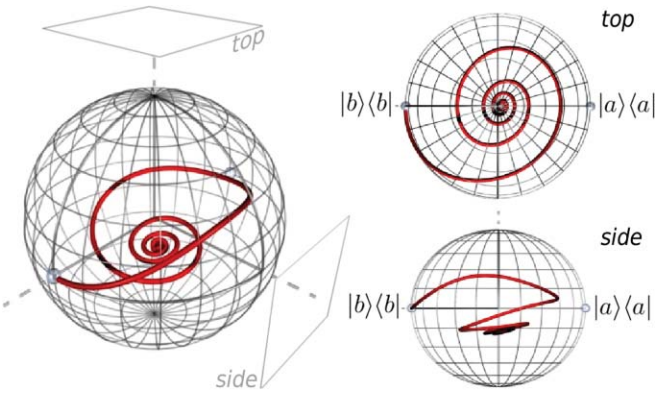

FIG. 3. Trajectory on the Bloch sphere of the dimer system for $\lambda = 10$ meV. The system undergoes a spiral trajectory to reach a mixed state located at the center of the Bloch sphere.

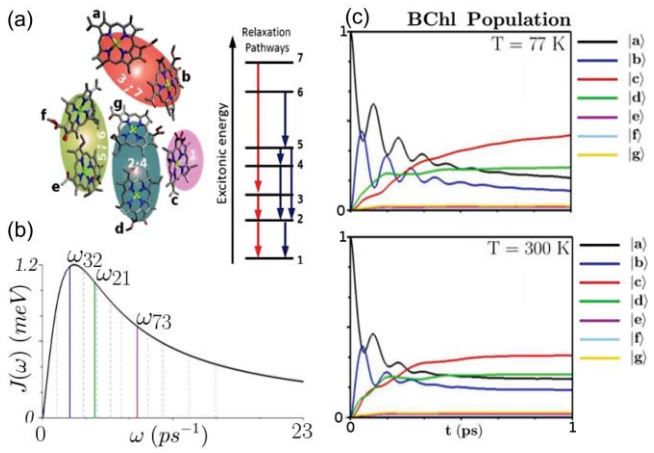

FIG. 4. (a) The 7 BChl of the FMO complex labeled from a to g. Due to the weak interactions between each BChl and the differences in their on-site energies the excitonic states, labeled from 1 to 7, are mainly localized on one or two BChl. Two relaxation pathways have been experimentally observed driving an initial excitation to the lowest lying excitonic state (Ref. 8). (b) Bath spectral density used to compute the relaxation dynamics. The three oscillation frequencies of the red relaxation pathway are located near the maximum of $\mathcal{J}(\omega)$. (c) The population oscillations obtained with the SSH algorithm show coherent oscillations lasting for almost 1 picosecond.

compact full picture of the evolution of a quantum system. The Bloch trajectory of the dimer system is represented in Fig. 3 for a reorganization energy of $\lambda = 10$ meV. Initially located at $|b\rangle\langle b|$, the system follows a spiral trajectory to reach a point located almost at the center of the sphere. This indicates a major loss of coherence during the evolution, since the trajectory enters the interior of the sphere. The asymptotic state is, therefore, not a coherent superposition of states that are located at the surface of the sphere, but rather a mixed state; since $\mathcal{Y} \simeq \mathcal{Z}(t) \simeq 0$. This decoherence is not introduced by a dephasing Hamiltonian as in the SH approach[28] but by the quantum jumps that disentangle the different parts of the system destroying the coherences progressively. This simple two-state situation both shows how to use the SSH scheme in a tight-binding formalism and provides some conceptual ideas that we carry forward to deal with the FMO complex.

III. COHERENT EXCITONIC TRANSFER IN THE FMO: THE INFLUENCE OF BCHL 8

Understanding the excitonic transfer in the FMO complex has been an intense field of study since the observation of the coherent oscillations in this compounds. These oscillations have been the source of speculation on the role of quantum coherence in energy transfer in biological compounds. Among other methods, the Lindblad equation[22] has been used, as have the reduced hierarchy equation approach[34] or the non-Markovian quantum jumps.[38] All these calculations have been performed on the FMO structure represented in Fig. 4(a) containing seven BChl labeled from a to g. The simplest exciton Hamiltonian of this system has been calculated using a numerical optimization of the Förster interaction terms in order to fit the absorbance spectra[16] and reads

$$\mathcal{H} = \sum_{x=a,\ldots,g} e_x |x\rangle\langle x| + \sum_{x,y} \alpha_{xy} |x\rangle\langle y|, \tag{11}$$

where $|x\rangle$ represents the state where the BChl x is in its S_1 state and all the other BChls are in their S_0 state. More elaborated models of the FMO complex have been studied[37] but would not be considered here. The numerical values of the on-site energies, e_x, and the coupling strength, α_{xy}, between two sites can be found in Ref. 16. In this model, the energy transfer is supposed to be initiated on BChl a or f that are the closest to the baseplate. Starting from one of these BChls, the exciton has to reach the BChl c located very close to the reaction center. The excitonic states, i.e., the eigenstates of the Hamiltonian (11) are also represented in Fig. 4(a) and are labeled from 1 to 7. Due to the weak couplings between the BChls and their relatively large on-site energy differences, these excitonic states are strongly localized on one or two BChls. Thus the target state, $|c\rangle$, contributes essentially to the lowest lying excitonic state $|1\rangle$ and the initial state $|a\rangle$ contributes mainly to $|3\rangle$ and weakly to $|7\rangle$. To evaluate the efficiency of exciton transfer, we introduce the simple function: $\mathcal{E} = (1/t_{max}) \int_0^{t_{max}} \langle c|\rho_S(\tau)|c\rangle d\tau$.[38] This function evaluates how much the target state of the evolution is populated during excitonic transport and is very useful to compare the relaxation of a given system as its interactions with its environment change. Due to the arbitrary choice of t_{max}, this efficiency is however hard to relate with experimental data. Besides, depending on the value of t_{max}, $\mathcal{E}$ grasps different characteristics of the excitonic transfer: when t_{max} is much larger than the relaxation time, $\mathcal{E}$ depends mainly on the maximum amplitude of the target state population. On the contrary, for shorter t_{max}, $\mathcal{E}$ depends strongly on the transfer rate, i.e., how fast this maximum population is reached. In the following, t_{max} is chosen as 1 ps to capture the early events of the exciton transfer and this gives a good picture of the transfer rate.

Experimental evidences suggest a structured relaxation pathway among the excitonic states.[6] Due to the overlapping between the excitonic states, the relaxation dynamics does not climb down the ladder of excitonic states step by step. Two different dominant relaxation pathways has been identified as represented in Fig. 4(a).[8] These two pathways are almost orthogonal and only the second excitonic states participates in both of them. These relaxation pathways are easily

integrated in the SSH algorithm in the $\mathcal{R}_S$ matrix. For example, the red pathway in Fig. 4(a) leads to the relaxation matrix: $\mathcal{R}_S = 1/2(|7\rangle\langle 3| + |3\rangle\langle 2| + |2\rangle\langle 1| + \text{c.c.})$. Once again even if all the transitions are equivalent in $\mathcal{R}_S$, their associated rates can be very different depending on the bath spectral density. This spectral density is given here by an OBO model with a reorganization energy λ of 10 meV and a cutoff frequency of $\omega_c = 3$ ps$^-$ which are typical values for photosynthetic systems.[34] This spectral density is represented in Fig. 4(b) with the oscillation frequencies corresponding to the transitions in the red relaxation pathway. These oscillation frequencies, ω_{73}, ω_{32}, and ω_{21}, are very close to the maximum of the $\mathcal{J}(\omega)$ leading to a fast decay from one excitonic state to another. Many other models can be used to define the bath spectral density and replace the rather simple one used here. Particularly, recent results point at the presence of many high frequency modes due to the internal vibrations of the BChls.[40,41] The impact of these modes on the relaxation dynamics is not addressed here, since due to the large difference between their intrinsic energies and the typical energy range of the FMO complex, these modes are supposed not to affect the dynamics significantly and are, therefore, ignored.

The population oscillations represented in Fig. 4(c) were obtained solving the FMO dynamics with the SSH algorithm, for $T = 77$ K and 300 K, with $\Lambda = 1.05$ to remain in the Markovian limit. Six modes were used to describe the bath and the dynamics was averaged over 500 realizations with a 0.5 fs time step. These oscillations are very similar to the ones obtained in the literature with different methods to simulate energy relaxation,[27] confirming the ability of the SSH method to deal with such systems. It is clearly seen that coherent oscillations are preserved up to a picosecond even at room temperature, as seen experimentally. These coherent oscillations occur between the local BChl states $|a\rangle$ and $|b\rangle$ due to their strong electronic coupling, 13 meV, and their weak energy difference, 25 meV. These oscillations have generated an extraordinary amount of discussion on the role of quantum coherence in biological systems. However, the population observed on the local BChl state $|c\rangle$ is not due to these coherent oscillations but to the relaxation process that progressively takes the initial excitation down to the lowest lying excitonic states, mainly localized on $|c\rangle$. Thanks to this relaxation scheme, the exciton transfer efficiency reaches $\mathcal{E} = 80 \times 10^{-3}$ for $T = 77$ K and $\mathcal{E} = 74 \times 10^{-3}$ for $T = 300$ K. If only a coherent evolution without any energy relaxation were considered, the population of $|c\rangle$ would remain almost null due to its large on-site energy difference with the initial state $|a\rangle$. Such a situation would lead to $\mathcal{E} \simeq 0$. Preserving the coherence may not necessarily enhance excitation propagation in the FMO complex that requires energy relaxation to go from $|a\rangle$ to $|c\rangle$.

The role of a eighth pigment in the FMO complex could bring new light on the question of the role of quantum coherence in exciton transfer. Whereas it has been thought for more than 30 years that each of the three identical subunits of the FMO complex contain seven BChl, a eighth BChl has recently been identified.[15] This new structure is represented in Fig. 5(a). The new BChl is located very close to the chlorosome, suggesting that it would be the entry point

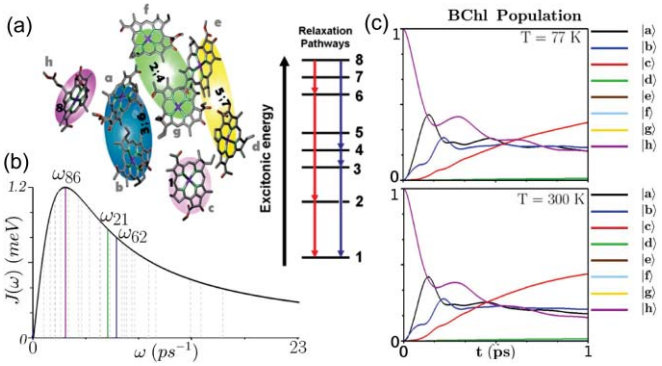

FIG. 5. (a) The eight BChl constituting the FMO complex. BChl h, close to the base plate, is the initial state of the evolution. BChl c, close to the reaction center, is the target state of the evolution. The relaxation among the delocalised excitonic states, noted from 1 to 8, drives the initial excitation following different possible pathways represented on the left. (b) Bath spectral density used to compute the relaxation dynamics. The oscillation frequencies of the transition composing the red relaxation pathway are located near the maximum of $\mathcal{J}(\omega)$. c) Population of the local BChl states starting from $|h\rangle$ and showing only weak coherent oscillations.

of the energetic flux through the FMO complex. However, this eighth BChl is rather far away from the other ones and interacts weakly with the rest of the subunit network.[17] Very recent studies suggest a stronger interaction between the eighth BChl and the neighboring monomer.[42] These intermonomer interactions are not considered in this article (to remain consistent with the seven site model used above where the dynamics have been solved within a given subunit). The simulation of the dynamics of the entire FMO complex including the three monomers and their interactions will be addressed in a future publication. In this article, we use the early model developed by Renger's group.[17] The on-site energies of the 7 BChls a to f, as well as their mutual interactions, are slightly different from the seven-site model used above leading to a different spatial delocalisation of the different eigenstates. In this model, the highest excitonic state is localized on the local BChl state, $|h\rangle$, and the lowest excitonic state is still localized on $|c\rangle$. The excitation has, therefore, to climb down all the excitonic ladder to go from its entry to its exit point. Adapting the red relaxation pathway of Fig. 4(a) to this new structure, one obtain the relaxation pathway represented in Fig. 5(a) where the initial excitation relaxes from the eighth to the sixth excitonic state then to the second one and finally reaches the lowest lying excitonic state, labeled 1. The relaxation matrix for this model therefore reads: $\mathcal{R}_S = 1/2(|8\rangle\langle 6| + |6\rangle\langle 2| + |2\rangle\langle 1| + \text{c.c.})$. Despite the more sophisticated models available, as discussed above, the spectral density of the bath used here follows an OBO model with a reorganization energy: $\lambda = 10$ meV and a cutoff frequency: $\omega_c = 3$ ps$^-$ in order to compare the results obtained with the 7 and 8 sites model of the FMO. This spectral density is represented in Fig. 5(b) with the oscillation frequencies corresponding to the transition composing the red relaxation pathway represented in Fig. 5(a) and used here. These frequencies lie around the maximum of $\mathcal{J}(\omega)$, leading once again to a fast relaxation between the excitonic states.

The SSH algorithm was used to compute the dynamics of this model using the red relaxation pathway of Fig. 5(a)

and the same parameters as previously: $T = 77$ K and 300 K and with $\Lambda = 1.05$. The bath was composed of 6 modes and 500 realizations have been computed to obtain the final dynamics with a 0.5 fs time step. The populations of the different BChls are plotted in Fig. 5(c). Due to the very weak coupling strength between BChl h and the rest of the BChl network, the long living coherent oscillations observed in Fig. 4(c) are far less important here. Due to this weak coupling, the first step in the evolution is not dominated by a coherent oscillation as in Fig. 4(c), but by an energy relaxation from the eighth to sixth excitonic state that prevents the coherences from attaining much amplitude. Despite this lack of coherence in the evolution, the relaxation dynamics is as efficient as in the previous case, reaching $\mathcal{E} = 110 \times 10^{-3}$ and $\mathcal{E} = 70 \times 10^{-3}$ for $T = 77$ K and 300 K. This suggests that coherent oscillations may not particularly enhance exciton transfer efficiency. In their recent work,[17] Busch *et al.* even go further, suggesting that the initial state of the evolution would rather be an excitonic state leading to a purely incoherent evolution among the excitonic states that nevertheless evolve efficiently to the final BChl.

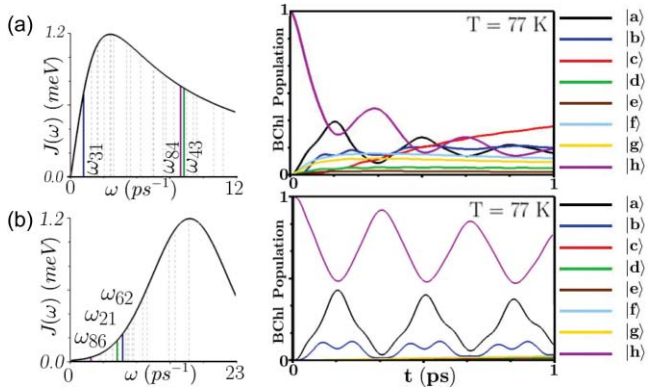

FIG. 6. (a) OBO spectral density with a cutoff frequency of $\omega_c = 3$ ps^{-1}. The three oscillations frequencies correspond to the three transitions involved in the blue relaxation pathway of Fig. 5(a). Due to the weak system-bath interaction this combination leads to long living coherent oscillations but to an inefficient exciton transfer. (b) Gaussian spectral density centered on $\omega_c = 16.5$ ps^{-1} and the three frequencies that correspond to the red relaxation pathway of Fig. 5(a). This leads to extremely weak system-bath interactions and suppresses the exciton transfer.

IV. ENGINEERING THE RELAXATION PATHWAYS

Supposing that quantum coherence preservation is not the only strategy to transfer energy efficiently, one can wonder what else can enhance or suppress this transfer. As we have seen in Figs. 4(b) and 5(b), the oscillation frequencies corresponding to the different transitions composing the relaxation pathways are very close to the maximum of the bath spectral density. It has been recently demonstrated that excitonic transfer can be directed to different target states depending on the interaction between these states and the bath.[39] To understand how the adaptation of the bath spectral density to the oscillation frequencies of the system modifies the excitonic transfer, two solutions can be implemented: one can change the transitions that comprise the relaxation pathway or keep the same transitions but using a different bath spectral density. This is what was done in Fig. 6 where the dynamics was solved for $T = 77$ K and in the Markovian limit ($\Lambda = 1.05$). The bath was composed of 6 modes and the evolution has been averaged over 500 realizations with a 0.5 fs time step.

Figure 6(a) corresponds the same OBO spectral density as in Fig. 5(b) but using the blue relaxation pathway shown in Fig. 5(a). The frequencies of the transition that compose of this relaxation pathway are very different from Fig. 5(b). The oscillation ω_{43} is the smallest one in the BChl network spectrum and lie in a spectral region where $\mathcal{J}(\omega)$ is relatively small. The two other oscillation frequencies, ω_{84} and ω_{31}, are larger than the cutoff frequency of the bath spectral density but also lies in a region where $\mathcal{J}(\omega)$ is relatively weak. Consequently all these frequencies lead to slow relaxation rates between the excitonic states. The populations of the BChls have been computed following the SSH approach using this relaxation pathway and are represented in Fig. 6(a). Due to the weak system-bath interaction discussed above, the transport efficiency from $|h\rangle$ to $|c\rangle$ is far less efficient than in Fig. 5(c) and equals: $\mathcal{E} = 46 \times 10^{-3}$. On the other hand, coherent oscillations are preserved up to a picosecond due to the slow relaxation rates but without enhancing exciton transport.

Figure 6(b) corresponds to a Gaussian bath spectral density centered on a high frequency, i.e., 16.5 ps^{-}. The transitions represented superposed by this bath spectral density correspond to the red relaxation pathway represented in Fig. 5(b). This model leads to extremely weak density of states around the oscillations frequencies, ω_{86}, ω_{62}, and ω_{21}, that form the relaxation pathway. The populations of the 8 BChls were computed with the SSH approach and are represented in Fig. 6(b). Excitonic transfer between $|h\rangle$ and $|c\rangle$ is completely suppressed leading to $\mathcal{E} = 0$. This inefficient transport is here due to a very bad adaptation of the bath spectral density to the relaxation pathway. However, benefiting from the slow relaxation rate, the evolution remains coherent for a very long time, leading to strong coherent oscillations.

The results presented in Fig. 6 could lead to the conclusion that the more important the spectral density the better exciton transfer. This simplistic deduction is wrong. Using an OBO model for $\mathcal{J}(\omega)$ and the red relaxation pathway shown in Fig. 5(a), the excitonic transport efficiency through the eight BChl, was calculated for different values of the reorganization energy, λ, and different cutoff frequencies, ω_c. The result of these calculations is represented in Fig. 7 for four different cutoff frequencies and for λ ranging from 1 to 50 meV. All the calculations have been made at T = 77 K, in the Markovian limit, i.e., $\Lambda = 1.05$, using six modes to describe the bath and averaging the final dynamics over 500 realizations.

As seen in Fig. 7, a large cutoff frequency leads to a $\mathcal{E}(\lambda)$ curve that presents a maximum which is progressively flattened when ω_c decreases. With $\omega_c = 5.8$ ps^{-1}, $\omega_c = 4.3$ ps^{-1}, and $\omega_c = 3$ ps^{-1}, excitonic transport is maximally efficient for a reorganization energy of $\lambda = 16$, 18, and 21 meV, respectively. For larger reorganization energies, this efficiency decreases due to the very fast relaxation rate that localizes the excitation on high energy excitonic states. The

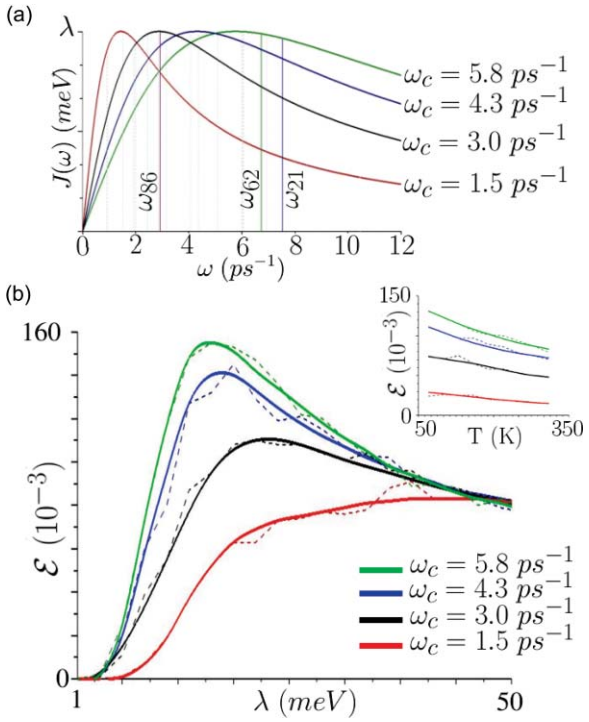

FIG. 7. (a) OBO bath spectral density for different values of the cutoff frequency ω_c. Depending on ω_c the three oscillation frequencies involved in the red relaxation pathway shown in Fig. 5, more or less strong system-bath interactions are obtained. (b) Excitonic transfer efficiency with respect of the reorganization energy λ and for different values of the cutoff frequency ω_c. The bath spectral density follows the model presented above. The dashed lines represent the exact numerical values obtained with the SSH algorithm and the plain line the best fit of these data.

case $\omega_c = 1.5$ ps^{-1} does not present a maximum and $\mathcal{E}(\lambda)$ simply increases with λ to reach its asymptotic value. The temperature dependence of the exciton transport efficiency is represented in the inset of Fig. 7(b), showing the decrease of $\mathcal{E}$ with T. This decrease is simply an equilibrium issue, due to the fact that the lowest excitonic state is less populated for high temperature than for low temperature.

Comparing the cases $\omega_c = 3$ ps^{-} and $\omega_c = 5.8$ ps^{-} is very informative. With $\omega_c = 3$ ps^{-}, the oscillation frequency ω_{86} is situated right on the maximum of $\mathcal{J}(\omega)$ and, therefore, the relaxation rate of the first transition in the exciton basis, i.e., from the eighth to the sixth excitonic state, is faster than the other transitions. But with $\omega_c = 5.8$ ps^{-1} the oscillation frequencies ω_{62} and ω_{21} correspond to the largest value of $\mathcal{J}(\omega)$. These two transitions, that are the last transitions in the relaxation pathway, are consequently the fastest during the relaxation dynamics. Besides, the fastest transitions lead to similar system-bath interactions in both configurations: $\mathcal{J}(\omega_{86})|_{\omega_c=3\text{ps}^{-1}} \simeq \mathcal{J}(\omega_{62})|_{\omega_c=5.8\text{ps}^{-1}} \simeq \mathcal{J}(\omega_{21})|_{\omega_c=5.8\text{ps}^{-1}}$. The same thing is true for the slow transitions:

$\mathcal{J}(\omega_{86})|_{\omega_c=5.8\text{ps}^{-1}} \simeq \mathcal{J}(\omega_{62})|_{\omega_c=3.0\text{ps}^{-1}} \simeq \mathcal{J}(\omega_{21})|_{\omega_c=3.0\text{ps}^{-1}}$. A large difference on the overall system-bath interactions cannot explain why exciton transfer is much more efficient with $\omega_c = 5.8$ ps^{-} than with $\omega_c = 3$ ps^{-}. This efficiency difference suggests that exciton transfer in a multitransitions relaxation pathway is enhanced when the relaxation rate of the first transition is slower than the relaxation rate of the following ones. Indeed, if the relaxation rate of first transition is very large, the evolution is localized and can not propagate along the system. But when the first transition is slower, the evolution can propagate longer before being localized by the system-bath interaction. The adaptation of the bath spectral density to the system not only requires that the transitions involved in the relaxation pathway lie in a region where the spectral density is high enough, but also that the early transitions in the relaxation pathway relax slower than the latter transitions. This opens the way to fine engineering of the relaxation pathway, accounting for this relaxation rate gradient among the transitions involved in the relaxation pathway.

V. CONCLUSION

The stochastic surrogate Hamiltonian has been applied to study the energy relaxation of systems whose Hamiltonians are defined on a discrete exciton basis set. This has been done to circumvent the grid propagation methods that are numerically expensive and, therefore, not well adapted to study large systems, such as photosynthetic complexes. The SSH has first been applied to model dimer systems where the combination of coherent oscillations and relaxation leads to damped oscillations as expected from the Redfield equation. For the SSH approach to converge to a Born-Markov approach, the bath modes must be frequently reset to their thermal states, and therefore requires a large value of Λ. The relaxation dynamics of the FMO complex have then been simulated using the SSH algorithm with the available tight-binding exciton models. With the seven-BChl model widely used in the literature, these calculations lead to long-living coherent oscillations between the local S_1 BChl states $|a\rangle$ and $|b\rangle$ as already observed and modeled elsewhere. These coherent oscillations have led to numerous hypothesis on the role of quantum coherence in biological systems. However the recent discovery of a eighth BChl in the structure of the FMO complex brings a new light on this specific question. This new BChl is close to the baseplate and is, therefore, the entry point of the excitonic transfer on the BChl network. However, due to its distance from the other BChls, this new pigment is only weakly coupled to the rest of the network. Because of this weak coupling, exciton transfer through the FMO shows almost no coherent oscillations. The first step of the transfer here is a relaxation from the highly excited excitonic state to lower ones and not a coherent oscillation between two BChls. Despite this lack of coherence in the dynamics, exciton transfer is actually more efficient in the eight-BChl structure than in the seven-BChl structure, where coherent oscillations were important. This implies that coherent oscillations may not be the key to enhance exciton transfer.

We have reached the intriguing conclusion that in addition to the proposed quantum coherence preservation, biological system can use a different strategy, based on the properties of the bath spectral density, to enhance or suppress exciton transfer. This transfer can be dramatically suppressed when the spectral density is low around the oscillation frequencies of the transitions involved in the relaxation pathway. This was shown by changing the relaxation pathway or the bath

spectral density. It seems that exciton transfer is enhanced when the relaxation pathway presents a gradient in the relaxation rate of the different transitions giving slower relaxation rates for the first transitions than for the last ones. If quantum tricks are used to transfer excitation efficiently, these tricks may be based on the adaptation of the bath spectral density to the transitions that form the relaxation pathway. These conclusions, drawn from a rather simple model system, have now to be confirmed using more sophisticated representations of the FMO BChl network and its environment. If confirmed with such models, this approach may open the way to a new route to design efficient artificial devices by engineering the interaction with their environment.

ACKNOWLEDGMENTS

We thank Gil Katz, Ronnie Kosloff, Greg Engel, Alan Aspuru Guzik, and especially Robert Blankenship for helpful remarks. This work was supported by the Non-equilibrium Energy Research Center (NERC) which is an Energy Frontier Research Center funded by the U.S. Department of Energy, Office of Science, Office of Basic Energy Sciences under Award Number DE-SC0000989 and by DARPA under Award Number N66001-10-1-4066 for the QuBE project.

[1]H. C. Longuet-Higgins, Biophys. J. **2**, 207 (1968).
[2]M. Arndy, T. Juffmann, and V. Vedral, HFSP J. **3**, 386 (2008).
[3]E. Schrodinger, *What is Life? The Physical Aspect of the Living Cell* (Cambridge University Press, Cambridge, England, 1944).
[4]T. Forster, Ann. Phys. **437**, 55 (1948).
[5]R. E. Fenna and B. W. Matthews, Nature (London) **258**, 573 (1975).
[6]T. Brixner, T. Mancal, I. V. Stiopkin, and G. R. Fleming, J. Chem. Phys. **121**, 4221 (2004).
[7]T. Brixner, J. Stenger, H. M. Vaswani, M. Cho, R. E. Blankenship, and G. R. Fleming, Nature (London) **434**, 625 (2005).
[8]G. S. Engel, T. R. Calhoun, E. L. Read, T.-K. Ahn, T. Mancal, Y. C. Cheng, R. E. Blankenship, and G. R. Fleming, Nature (London) **446**, 782 (2007).
[9]E. Collini, C. Y. Wong, K. E. Wilk, P. M.G. Curmi, P. Brumer, and G. D. Scholes, Nature (London) **463**, 644 (2010).
[10]J. Strümpfer and K. Schulten, J. Chem. Phys. **131**, 225101 (2009).
[11]T. R. Calhoun, N. S. Ginsberg, G. S. Schlau-Cohen, Y.-C. Cheng, M. Ballottari, R. Bassi, and G. R. Fleming, J. Phys. Chem. B **113**, 16291 (2009).
[12]M. Mohseni, P. Rebentrost, S. Lloyd, and A. Aspuru-Guzik, J. Chem. Phys. **129**, 174106 (2008).
[13]S. Lloyd, Nat. Phys. **5**, 164 (2009).
[14]V. L. Gunderson, S. M. Mickley, and M. R. Wasielewski, Chem. Commun. **46**, 401 (2010).
[15]D. E. Tronrud, J. Wen, L. Gay, and R. E. Blankenship, Photosynth. Res. **100**, 79 (2009).
[16]J. Adolphs and T. Renger, Biophys. J. **91**, 2778 (2006).
[17]M. S. Busch, F. Muh, M. E. A. Madjet, and T. Renger, J. Phys. Chem. Lett. **2**, 93 (2011).
[18]H. P. Breuer and F. Petruccione, *The Theory of Open Quantum System* (Oxford University Press, New York, 2002).
[19]S. Nakajima, Prog. Rep. Theor. Phys. **20**, 948 (1958).
[20]R. Zwanzig, J. Chem. Phys. **33**, 1338 (1960).
[21]A. Ishizaki and G. R. Fleming, J. Chem. Phys. **130**, 234110 (2009).
[22]B. Palmieri, D. Abramavicius, and S. Mukamel, J. Chem. Phys. **130**, 204512 (2009).
[23]D. Egorova, A. Kuhl, and W. Domcke, Chem. Phys. **268**, 105 (2001).
[24]K. Dietz, J. Phys. A **36**, 5595 (2003).
[25]J. Dalibard, Y. Castin, and K. Molmer, Phys. Rev. Lett **68**, 580 (1992).
[26]J. Pillo, K. Härkönen, S. Maniscalco, and K.-A. Suominen, Phys. Rev. A **79**, 062112 (2009).
[27]A. Ishizaki and G. R. Fleming, J. Chem. Phys. **130**, 234111 (2009).
[28]C. P. Koch, T. Kluner, and R. Kosloff, J. Chem. Phys. **116**, 7983 (2002).
[29]C. P. Koch, T. Kluner, H.-J. Freund, and R. Kosloff, Phys. Rev. Lett. **90**, 117601 (2003).
[30]G. Katz, R. Kosloff, and M. A. Ratner, J. Chem. Phys. **129**, 034108 (2008).
[31]G. Katz, R. Kosloff, and M. A. Ratner, New J. Phys. **12**, 015003 (2010).
[32]E.-M. Laine, J. Piilo, and H.-P. Breuer, Phys. Rev. A **81**, 062115 (2010).
[33]D. Gelman and R. Kosloff, Chem. Phys. Lett. **381**, 129 (2003).
[34]A. Ishizaki and G. R. Fleming, Proc. Natl. Acad. Sci. U.S.A. **106**, 17255 (2009).
[35]S. Mukamel, *Principles of Nonlinear Optics and Spectroscopy* (Oxford University Press, New York, 1995).
[36]R. Mosseri and R. Dandoloff, J. Phys. A **34**, 10243 (2001).
[37]D. Arbamavicius and S. Mukamel, Proc. Natl. Acad. Sci. U.S.A. **105**, 8525 (2008).
[38]P. Rebentrost, R. Chakraborty, and A. Aspuru-Guzik, J. Chem. Phys. **131**, 184102 (2009).
[39]A. Pedromo, L. Vogt, A. Namaje, and A. Aspuru-Guzik, Appl. Phys. Lett. **96**, 093114 (2010).
[40]D. Abramavicius and S. Mukamel, J. Chem. Phys. **133**, 184501 (2010).
[41]V. I. Novoderezhkin, J. P. Dekker, and R. van Grondelle, Biophys. J. **93**, 1293 (2007).
[42]C. Olbrich, T. L. C. Jansen, J. Liebers, M. Aghtar, J. Strümpfer, K. Schulten, J. Knoester, and U. Kleinekathüfer, J. Phys. Chem. B **115**, 8609 (2011).